Journal of Biomechanics 46 (2013) 2075–2081

Contents lists available at SciVerse ScienceDirect

Journal of Biomechanics

journal homepage: www.elsevier.com/locate/jbiomech
www.JBiomech.com

Mechanical analysis of ovine and pediatric pulmonary artery for heart valve stent design

M.S. Cabrera [a,*], C.W.J. Oomens [a], C.V.C. Bouten [a], A.J.J.C. Bogers [b], S.P. Hoerstrup [c,d], F.P.T. Baaijens [a]

[a] Department of Biomedical Engineering, Eindhoven University of Technology, Eindhoven, The Netherlands
[b] Heart Valve Bank Rotterdam, Department of Cardiothoracic Surgery, Erasmus MC, Rotterdam, The Netherlands
[c] Department of Surgical Research, University of Zürich, Zurich, Switzerland
[d] Clinic for Cardiovascular Surgery, University Hospital Zürich, Zurich, Switzerland

ARTICLE INFO

Article history:
Accepted 28 April 2013

Keywords:
Pulmonary artery
Heart valve replacement
Biaxial tensile test
Pediatric stent design
Constitutive modeling

ABSTRACT

Transcatheter heart valve replacement is an attractive and promising technique for congenital as well as acquired heart valve disease. In this procedure, the replacement valve is mounted in a stent that is expanded at the aimed valve position and fixated by clamping. However, for this technique to be appropriate for pediatric patients, the material properties of the host tissue need to be determined to design stents that can be optimized for this particular application. In this study we performed equibiaxial tensile tests on four adult ovine pulmonary artery walls and compared the outcomes with one pediatric pulmonary artery. Results show that the pediatric pulmonary artery was significantly thinner (1.06 ± 0.36 mm (mean $\pm$ SD)) than ovine tissue (2.85 ± 0.40 mm), considerably stiffer for strain values that exceed the physiological conditions (beyond 50% strain in the circumferential and 60% in the longitudinal direction), more anisotropic (with a significant difference in stiffness between the longitudinal and circumferential directions beyond 60% strain) and presented stronger non-linear stress–strain behavior at equivalent strains (beyond 26% strain) compared to ovine tissue. These discrepancies suggest that stents validated and optimized using the ovine pre-clinical model might not perform satisfactorily in pediatric patients. The material parameters derived from this study may be used to develop stent designs for both applications using computational models.

1. Introduction

Congenital heart defect affects between 4 and 10 out of every 1000 newborns (Marelli et al., 2007). Of these, 2.3 per 1000 live births require invasive surgery or result in death in the first year of life (Roger et al., 2011). Transcatheter valve replacement is gaining momentum and may be applicable for pediatric patients as well. The stent system plays a crucial role in this technology providing support and allowing fixation of the replacing heart valve. However, for heart valve replacement in pediatric patients, the stent must adapt and have the capacity to accommodate growth and allow remodeling of the artery. Percutaneous pulmonary and aortic valve replacement pre-clinical trials have been conducted with the use of self-expanding stents (Metzner et al., 2010; Attmann et al., 2005; Laborde et al., 2005; Ussia et al., 2010) with the ovine animal model being the preferred model for in vivo preclinical assessment.

Several experimental studies have been conducted to determine and model the mechanical properties of human (Sommer and Holzapfel, 2012), porcine (Zhao et al., 2011), lapine (Auricchio et al., 2001), vituline (Kao et al., 2011) and ovine arteries (Pham and Sun, 2012) by means of uniaxial and biaxial tensile tests. Self-expanding stents have also been analyzed computationally for use in carotid arteries (Conti et al., 2009; Wu et al., 2007). However, only a few studies concerning computational models of valve stents have been published (Tzamtzis et al., 2013; Schievano et al., 2010; Kumar and Mathew, 2008) and none of these included stents for pediatric applications. Furthermore, computational stent analyses for heart valve replacement only included experimental results to model aortic arteries (Wang et al., 2012; Sirois et al., 2011). However, until now, no stent analysis incorporated the mechanical properties of human or ovine pulmonary arteries, even though this information is available for human adult tissue (Azadani et al., 2011). To properly study stent materials and designs, a suitable representation of the vessel properties of the pediatric patient as well as the preferred animals (sheep) used in pre-clinical trials is required. The lack of information regarding the mechanical properties of ovine tissue (Pham and Sun, 2012;

* Corresponding author. Tel.: +31 40 247 3047; fax: +31 40 244 7355.
E-mail address: M.S.Cabrera@tue.nl (M.S. Cabrera).

0021-9290/$ - see front matter © 2013 Elsevier Ltd. All rights reserved.
http://dx.doi.org/10.1016/j.jbiomech.2013.04.020

Alastrué et al., 2008), more particularly the absence of studies on the pulmonary and aortic root mechanics, has limited the creation of representative computational models for testing stent designs for pre-clinical trials of heart valve prostheses. Therefore, the objective of this research was to determine the mechanical properties of ovine pulmonary roots, within and beyond the physiological range of stretch, to develop a constitutive model for finite element analysis of stents for pulmonary valve replacement. Despite the difficulty in obtaining human pediatric tissue, one pulmonary artery of an 8-month old infant was also tested.

2. Materials and methods

Supra-valvular segments of ovine pulmonary arteries were harvested within 2 h after death from the hearts of four white alpine adult sheep (number of samples=9-6-6-10, 3 years old, 70 ± 5 kg) at Zurich University Hospital. All animals received human care and the study was approved by the ethics committee (Veterinäramt, Gesundheitsdirektion, Kanton Zürich [197/2012]) in compliance with the Guide for the Care and Use of Laboratory Animals, published by the National Institutes of Health (NIH publication No. 85-23). The tissue was stored in phosphate buffered saline solution (PBS), cooled and transported to Eindhoven University of Technology for biaxial tensile testing within 4 days of harvesting. One pediatric pulmonary homograft (containing the valve leaflets, sub-valvular myocardial tissue and supra-valvular vascular wall) was obtained from a Dutch postmortem donor (number of samples=7, 8 months old), for whom permission for research was given. The homograft, which was assessed to be unfit for implantation but structurally intact, was obtained from the Heart Valve Bank Rotterdam (Erasmus University Medical Center, Rotterdam, The Netherlands). The tissue was stored at −80 °C until use. The valve was thawed according to the guidelines of the Heart Valve Bank Rotterdam. Briefly, the package containing the cryopreserved homograft was gently agitated in warm saline (± 40 °C) to dissolve ice-crystals and soften the graft. After thawing, the package containing the valve was opened and contents were deposited in a bowl. Cold phosphate buffered saline (PBS; Sigma) was gently added to allow the dimethyl sulfoxide (DMSO) to dilute from the tissue into the solution. After thawing, any visible fat or loose connective tissue was removed from the surface of the arterial wall before sectioning. An arterial ring was obtained from the region between the sinotubular junction artery and the bifurcation (more than 2 cm above the sinuses in the ovine case, right above the sinuses in the pediatric case due to the small size of the artery). The ring was cut open along its length and divided into two arterial segments using a custom-made cutter consisting of two parallel razor blades that were positioned in accordance with the circumferential direction of the artery (Christie and Barratt-Boyes, 1995; Lally et al., 2004). A maximum of ten square samples for biaxial mechanical testing were cut from each ring (Fig. 1) taking care to align the cutting device in the longitudinal direction of the artery to obtain the mechanical properties with respect to the anatomical directions. The thickness was measured at three locations with a caliper (Mitutoyo, CD-15 CPX) mounting the samples on a glass slide. Each sample was marked to indicate its circumferential orientation and stored in PBS at 4 °C until testing.

2.1. Biaxial tensile testing

Graphite particles were deposited with a cotton swab on the inner surface of the artery for optical strain measurements. The circumferential (θ) and longitudinal (L) directions of the arterial tissue were aligned with the stretching directions in a biaxial tensile tester (CellScale, Waterloo, Canada). The distance between clamps was set to $L_{\theta 0} = L_{L0} = L_0 = 3.5$ mm. Ten preconditioning cycles were applied uniaxially in both directions to a maximum stretch of 55% to reduce tissue hysteresis. Displacement-controlled equibiaxial protocols were implemented with a constant rate of L_0 mm/min. Consecutive cycles were performed, increasing the stretch by 10% between cycles (Fig. 2), until the tissue began to tear at the attachments. Testing was performed at ambient temperature and specimens were moistened throughout the test with PBS. A high resolution CCD camera registered real-time displacements during each loading cycle.

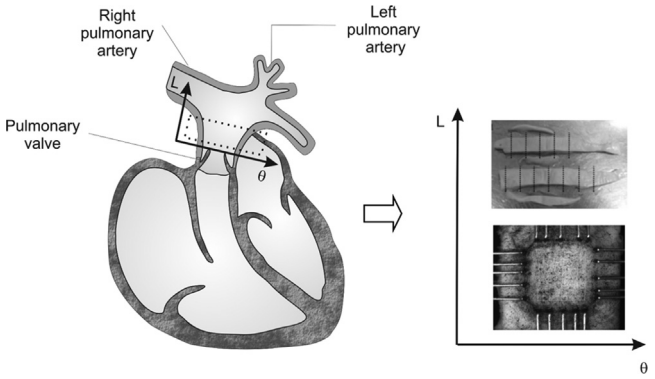

Fig. 1. Sample preparation for biaxial tensile testing.

Arteries were assumed to be incompressible and a plane stress situation was considered. Taking this into account, the experimental Cauchy stresses $\sigma_{i_{exp}} (i = \theta, L)$ were calculated with the forces F_i and sample dimensions obtained from the biaxial test (L_i and L_{i0} represent the distance between the clamps before and after applying a stretch $\lambda_i = L_i/L_{i0}$, respectively and t is the original thickness of the sample).

$$\sigma_{\theta_{exp}} = \frac{F_\theta \, \lambda_\theta}{L_{L0} \, t} \quad \sigma_{L_{exp}} = \frac{F_L \, \lambda_L}{L_{\theta 0} \, t} \tag{1}$$

The displacements of the marker coordinates of a 5×5 element grid were tracked through the loading cycle and exported (Labjoy 8.1) for Green-Lagrange strain tensor calculations (Geers et al., 1996) in MATLAB (R2010a, The MathWorks Inc., Natick, Massachusetts). The Green strain computed for all our plots and calculations is the strain in the midpoint of the grid. The relationship between the Green strain ε_i and the stretch λ_i is expressed by Eq. (2).

$$\varepsilon_i = \frac{1}{2}(\lambda_i^2 - 1) \tag{2}$$

2.2. Estimation of the physiological stress and stretch conditions in the in vivo state

Considering the artery as a cylindrical entity subjected to uniform internal pressure, the physiological stresses $\sigma_{i_{physio}}$ were estimated from the mean arterial pressure P and the radius r and thickness t of the artery at zero load state (Fukui et al., 2005; Azadani et al., 2011) according to Laplace's law for a thin walled cylinder.

$$\sigma_{\theta_{physio}} = \frac{Pr}{t} \quad \sigma_{L_{physio}} = \frac{Pr}{2t} \tag{3}$$

The mean arterial pressure was calculated from the systolic P_s and diastolic P_d pressures using the classic rule of thumb which has been demonstrated to provide a precise estimate of the mean pulmonary artery pressure in adults (Chemla et al., 2009).

$$P = P_d + \frac{(P_s - P_d)}{3} \tag{4}$$

The corresponding physiological strains $\varepsilon_{i_{physio}}$ and stretches $\lambda_{i_{physio}}$ were obtained by intersecting $\sigma_{i_{physio}}$ with the stress–strain curves of the equibiaxial tensile tests and applying Eq. (2). As indexes of the physiological condition in the in vivo state, the mean stress σ_m, mean strain ε_m and mean stretch λ_m are defined by

$$\sigma_m = \frac{\sigma_{\theta_{physio}} + \sigma_{L_{physio}}}{2} \quad \varepsilon_m = \frac{\varepsilon_{\theta_{physio}} + \varepsilon_{L_{physio}}}{2} \quad \lambda_m = \frac{\lambda_{\theta_{physio}} + \lambda_{L_{physio}}}{2} \tag{5}$$

2.3. Stiffness calculation

Differences in stiffness were evaluated by means of the secant modulus at diverse values of strain. Stiffness values were compared between species (in the longitudinal and circumferential directions) and per direction (ovine vs. pediatric tissue).

2.4. Constitutive modeling

The artery was assumed to be non-linear, hyperelastic and anisotropic. The Holzapfel–Gasser–Ogden (HGO) model (Gasser et al., 2006) was used to fit the biaxial experimental data. The model consists of a non-collagenous ground matrix represented by an incompressible neo-Hookean material. The anisotropic contribution is related to the fiber-reinforced nature of the material. Two families of fibers are embedded in the tissue and distributed with rotational symmetry about a mean direction. The strain energy density function (Eq. (6)) is represented by ψ where $c > 0$ and $k_1 > 0$ are stress-like material parameters, $I_1 = tr\mathbf{C}$ represents the first invariant of the symmetric right Cauchy–Green deformation tensor $\mathbf{C}$, $k_2 > 0$ is a dimensionless material parameter and $\kappa (0 \le \kappa \le 1/3)$ describes the level of dispersion in the fiber direction. $I_{4\alpha\alpha}$ are pseudo-invariants of $\mathbf{C}$ and the mean preferred directions of the fiber families ($\vec{A}_\alpha$ and $\vec{A}_\beta$) and ϕ is the angle of the fiber families with respect to the circumferential direction.

$$\psi = \frac{1}{2} c(I_1 - 3) + \frac{k_1}{2k_2}\left[\exp(k_2 E_1^2) - 1 + \exp(k_2 E_2^2) - 1\right] \tag{6}$$

$$E_{\alpha = 1,2} = \kappa(I_1 - 3) + (1 - 3\kappa)(I_{4\alpha\alpha} - 1) \tag{7}$$

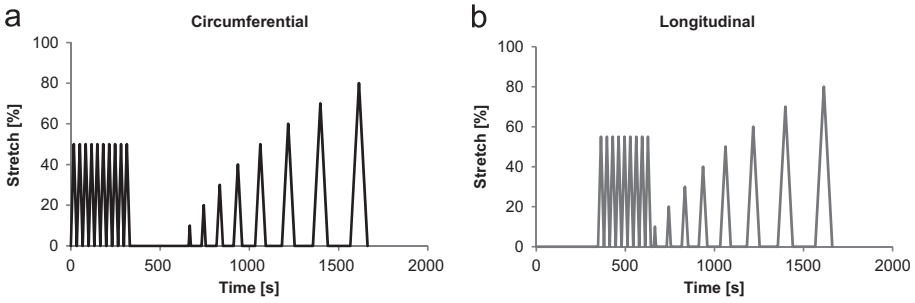

Fig. 2. Loading protocol for biaxial tensile testing in (a) circumferential and (b) longitudinal directions.

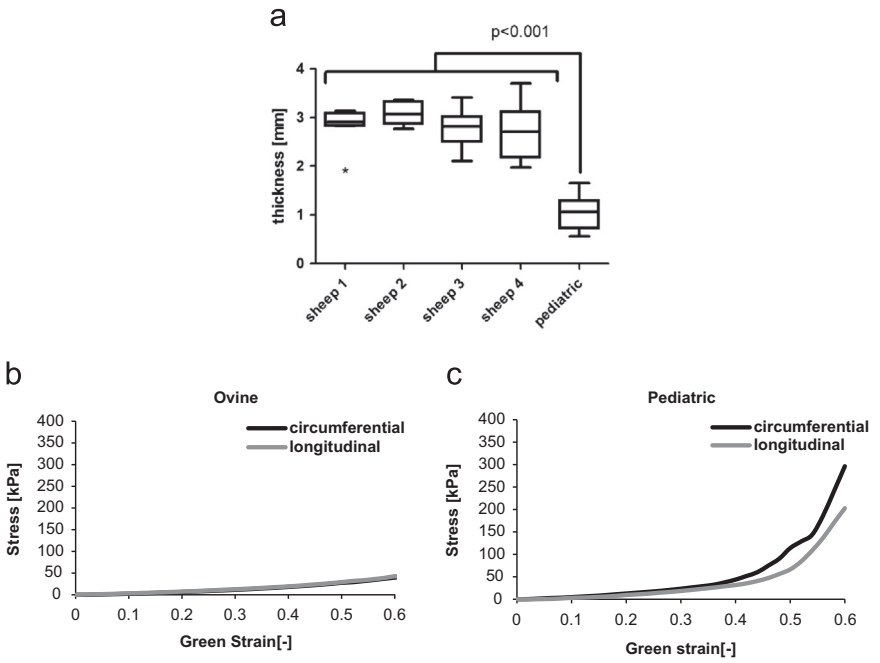

Fig. 3. Experimental results: (a) thickness, (b) stress–strain plots of ovine tissue at 80% biaxial stretching and (c) stress–strain plots of pediatric tissue at 70% biaxial stretching. The pediatric tissue is thinner, more anisotropic and presents a stronger non-linear stress–strain behavior at equivalent strains compared to ovine tissue.

$$I_{4\alpha\alpha} = \vec{A}_{\alpha} \cdot \not{c} \cdot \vec{A}_{\alpha} = f(\varphi) \tag{8}$$

From the strain energy density function, the numerical Cauchy stresses in the circumferential and longitudinal directions ($\sigma_{\theta_{num}}$ and $\sigma_{L_{num}}$) were derived considering that the material is incompressible, in a plane stress state and satisfies the stress equations in the principal strain directions:

$$\sigma_{i_{num}} = \lambda_i \frac{\partial \psi}{\partial \lambda_i} \tag{9}$$

Considering Eqs. (6)–(9) the resulting numerical stress–strain relationships are expressed by

$$\sigma_{\theta_{num}} = c(\lambda_\theta^2 - \tfrac{1}{\lambda_\theta^2 \lambda_L^2}) + 4k_1 E_1 \exp(k_2 E_1^2)\left[\kappa(\lambda_\theta^2 - \tfrac{1}{\lambda_\theta^2 \lambda_L^2}) + [(1-3\kappa)\lambda_\theta^2 \cos^2\varphi]\right.$$
$$\sigma_{L_{num}} = c(\lambda_L^2 - \frac{1}{\lambda_\theta^2 \lambda_L^2}) + 4k_1 E_1 \exp(k_2 E_1^2)\left[\kappa(\lambda_L^2 - \frac{1}{\lambda_\theta^2 \lambda_L^2})\right] + \left[(1-3\kappa)\lambda_L^2 \sin^2\varphi\right] \tag{10}$$

MATLAB subroutines were developed for extracting the experimental data, calculating the stresses and stretches, curve discretization and data fitting.

From Eqs. (1) and (10), the function to minimize was calculated as follows:

$$\chi^2 = \sum_{i=1}^{n} [(\sigma_{\theta_{\exp}} - \sigma_{\theta_{num}})^2 + (\sigma_{L_{\exp}} - \sigma_{L_{num}})^2] \tag{11}$$

where n is the number of points of each experimental curve. The constitutive parameters related to the mechanical properties (c, k_1 and k_2) were fitted to the experimental data using the Levenberg–Marquardt method for multivariate non-linear regression. There are two other unknown parameters related to the structure (ϕ and κ). In this study only ϕ participated in the fitting procedure and the dispersion parameter κ adopted six different values according to the (transversely isotropic) von Mises distribution of the collagen fibers $\kappa = 0, \frac{1}{15}, \frac{2}{15}, \frac{1}{5}, \frac{4}{15}, \frac{1}{3}$ (Gasser et al., 2006). The lower value of κ describes ideally aligned fibers, whereas the higher value represents isotropic distribution. Correlation was determined using the Pearson's correlation coefficient (r).

2.5. Statistical analysis

For statistical analysis, the normal distribution of the thickness measurements for ovine and pediatric tissue was verified by the Kolmogorov–Smirnov test. One-way ANOVA tests followed by Tukey's multiple comparison tests were used to compare the thickness among ovine and pediatric tissue. Two-way ANOVA tests were used to compare differences in stiffness. A probability value less than 0.05 was considered statistically significant. Statistical analyses were performed using GraphPad Prism (version 5.04 for Windows, GraphPad Software, San Diego California USA). All the values of measurements are presented as mean ± standard deviation.

3. Results

3.1. Tissue thickness and biaxial tensile tests

The thickness of all ovine and human samples was determined. One data set did not pass the normality test due to the presence of one observation that was numerically distant from the mean value (sheep 1, Fig. 3a). With an exception of this outlier, all data were normally distributed presenting no significant differences among

the ovine subjects ($p=0.3790$). On the other hand, the difference in thickness between pediatric (1.06 ± 0.36 mm) and ovine tissue (2.85 ± 0.40 mm) was found significant ($p < 0.001$).

Ovine tissue was tested up to an equibiaxially applied stretch of 80% and human tissue up to 70% since tissue tearing was evident for higher displacements. In all cases, ovine tissue showed an isotropic response (Fig. 3b) with circumferential and longitudinal curves overlapping. Moreover, the stress–strain behavior of ovine tissue was nearly linear in the measured range. Conversely, pediatric tissue (Fig. 3c) was less isotropic and stiffer than ovine tissue. The stress–strain behavior of pediatric tissue was clearly non-linear in both directions with a slow but abrupt transition from the low stiffness region to the high stiffness portion of the curve.

3.2. Estimation of the physiological conditions in the in vivo state

Systolic and diastolic pulmonary pressures were measured for all sheep by invasive methods ($18.25 \pm 4.35/16 \pm 4$ mmHg) and the mean arterial pressure was calculated from Eq. (4). Normal systolic and diastolic values of pulmonary pressure in human adults were found in literature (Watanabe et al., 2002). Considering that the mean pulmonary arterial pressure reaches the adult level two weeks after birth (Gao and Raj, 2010), these values are applicable for the pediatric case. Physiological stresses in both cases were calculated from Eq. (3) assuming an arterial radius of 12.5 mm in the ovine case and 11 mm in the pediatric case. Results are shown in Table 1.

The stress–strain average curves (Fig. 4) were intersected with the calculated physiological stresses to obtain the physiological longitudinal and circumferential strains. The corresponding stretches where calculated according to Eq. (2). Results are shown in Table 2. Finally the mean physiological stretches (Eq. (5)) were plotted over the stress-stretch plots for comparison. The transition strains between low and high stiffness regions were estimated by fitting each stress–strain curve with a seventh order polynomial and finding the local maximum in the function curvature (Madhavan et al., 2010). Results seem to show that for both ovine and pediatric tissue, the transition points of the stress-stretch curves are located beyond physiological range in both directions.

Table 1
Systolic, diastolic and mean pressure and the corresponding physiological circumferential, longitudinal and mean stresses for ovine and human pediatric tissue. Values are presented as mean ± standard deviation.

Tissue type	P_S [kPa]	P_d [kPa]	P	$\sigma_{\theta_{physio}}$ [kPa]	$\sigma_{L_{physio}}$ [kPa]	σ_m
Ovine	2.4 ± 0.6	2.1 ± 0.5	2.2 ± 0.4	9.6 ± 2.2	4.8 ± 1.1	7.2 ± 1.2
Pediatric	2.9 ± 1.4	1.0 ± 0.7	1.7 ± 0.7	8.7 ± 4.6	4.3 ± 2.3	6.5 ± 2.63

3.3. Stiffness estimation

Changes in stiffness were evaluated by means of the secant modulus at diverse values of strain. No statistically significant differences were evidenced when comparing the stiffness (Fig. 5a) in the longitudinal and circumferential directions of ovine tissue. However, major discrepancies were found in human tissue (Fig. 5b) for the last strain increment ($p < 0.01$) beyond physiological values. In addition, remarkable differences were encountered when comparing the stiffness of ovine and pediatric tissue in both directions (Fig. 6). Pediatric tissue was drastically stiffer than ovine tissue for diverse strain levels ($p < 0.0001$). These discrepancies were not found significant when strain was close to physiological values.

3.4. Data fitting

The material parameters that define the numerical Cauchy stresses defined by Eq. (11), for different values of fiber dispersion are shown in Table 3. All the experimental results, for ovine and pediatric tissue, respectively, were fitted simultaneously (Fig. 7). The quality of the fitting is estimated by comparing each numerical curve with the mean experimental curve for each tissue. In all cases, the numerical approximation was in close accordance with the experimental results. The best fitting was obtained considering the ovine tissue as completely isotropic, whereas for the pediatric tissue the degree of anisotropy is slightly higher.

4. Discussion

In this study we analyzed the mechanical properties of ovine and pediatric pulmonary tissue by performing equibiaxial tensile tests. Considerable discrepancies were found when comparing the mechanical properties of ovine and pediatric pulmonary walls. Pediatric tissue was found to be non-linear, stiffer, less isotropic and significantly thinner than ovine tissue. These differences will bring consequences when designing stents. It is likely that a stent that is validated and optimized using ovine pre-clinical testing needs to be redesigned for pediatric tissues because of the effect that material properties, thickness and dimensions will have on the arterial response to pressure and stent deployment. We also

Table 2
Circumferential, longitudinal and mean strains and stretches for ovine and human pediatric tissue.

Tissue type	$\varepsilon_{\theta_{physio}}$	$\varepsilon_{L_{physio}}$	ε_m	$\lambda_{\theta_{physio}}$	$\lambda_{L_{physio}}$	λ_m
Ovine	0.26	0.14	0.20	1.23	1.13	1.18
Pediatric	0.16	0.13	0.14	1.15	1.12	1.14

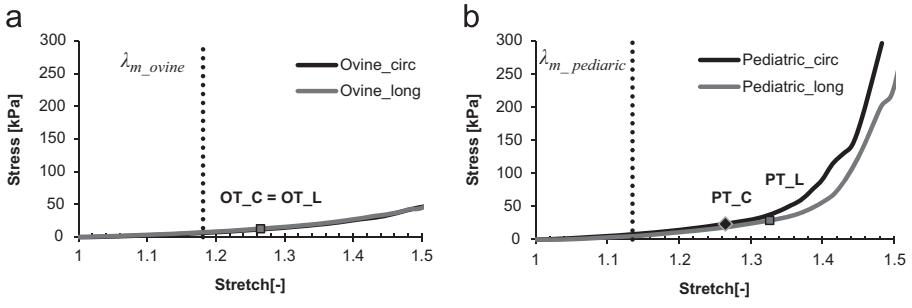

Fig. 4. Average experimental stress-stretch curves in the circumferential and longitudinal directions, transition points and mean physiological stretches in (a) ovine, and (b) pediatric tissue. In both cases the transition points (OT_C, OT_L, PT_C and PT_L) are located beyond physiological range in both directions.

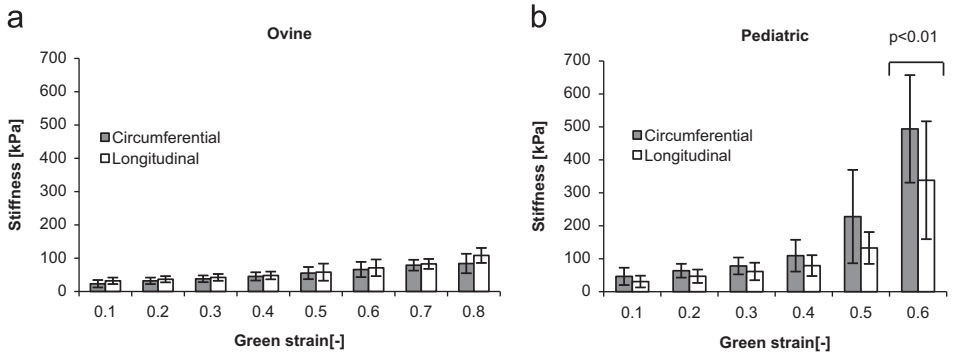

Fig. 5. Stiffness (secant modulus) in the circumferential and longitudinal directions (a) ovine and (b) pediatric. Major discrepancies were found in human tissue for the last strain increment beyond physiological values.

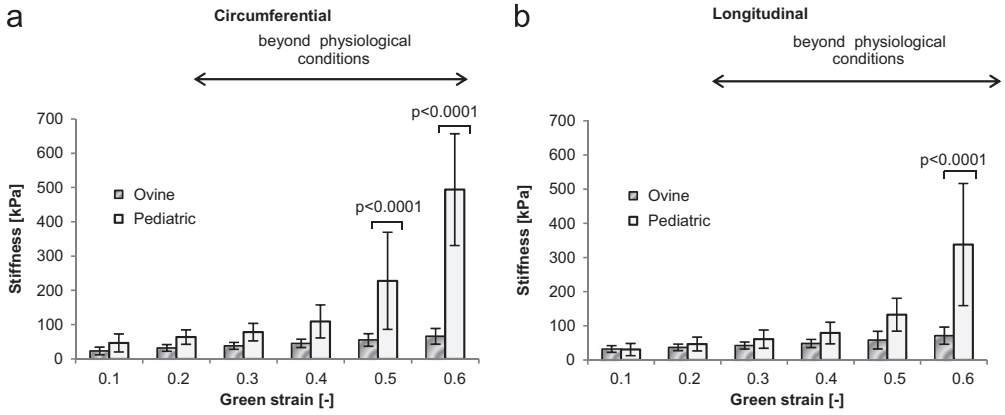

Fig. 6. Stiffness (secant modulus) of ovine and pediatric pulmonary tissue (a) circumferential and (b) longitudinal directions. The most significant differences between pediatric and ovine tissue are evidenced for strain values higher than the estimated physiological range.

showed that the most significant differences between pediatric and ovine tissue are seen for strain values higher than the estimated physiological range. The presence of the stent interacting with the artery represents a situation beyond physiological conditions and therefore there is a need to properly characterize arterial behavior under this scenario. For these reasons we believe that an independent arterial representation, characterized for conditions beyond physiological loading, is necessary for pediatric stent design. Nevertheless, the properties described in the present paper enable to perform the necessary finite elements simulations on stents for both ovine pre-clinical trials and pediatric applications.

In accordance with Pham and Sun (2012) we underline the need of having appropriate animal models to evaluate prostheses performance for future use in humans. Azadani et al. (2011) reported the mechanical properties of human adult pulmonary arteries (50 ± 12 years). The comparison between the mechanical behavior obtained in the present work for human pediatric arteries and the adult pulmonary arteries reported by Azadani is in accordance with the study by Gozna et al. (1974) showing a clear stiffer tendency in the adult case. On the other hand, this suggests that human adult tissue is even less likely to be comparable to the ovine tissue tested in this study. Pham and Sun (2012) also observed significant differences between aged human and ovine tissue when studying the mechanical properties of coronary sinus vessels.

The limitations of this investigation mainly relate to the reduced number of tissues tested, especially the single human pulmonary artery. In addition, the age of the sheep might not be optimal for a comparison with human pediatric tissue. As a consequence of aging, the mechanical properties of human arteries are known to differ (Gozna et al., 1974). Besides, biochemical changes in the collagen and elastin networks are known to occur with age (Stephens and Grande-Allen, 2007). For a more specific comparison with pediatric tissue, juvenile sheep would have been preferable. Fata et al. (2013) recently reported moderate changes in the regional mechanical properties of ovine pulmonary arteries with growth, no changes in thickness and a vessel diameter enlargement that suggests an increase of 40% in the wall stress. These differences should be taken into account in animal studies and computational models if both scenarios want to be combined for stent design optimization. On the other hand, acquiring fresh pediatric material is extremely difficult. Moreover, juvenile sheep are used for implantation and follow-up of valve stents and by the time of explantation, their age is already

Table 3
Material constants for the HGO model in ovine and pediatric tissue for diverse dispersion values.

Tissue type	κ	c [kPa]	k_1 [kPa]	k_2	φ [°]	r^2
Ovine	1/3	4.2	21.9	0	21	0.99
	4/15	2.2	17.5	0	50	0.99
	1/5	0.4	14.3	0.01	47	0.99
	2/15	0	10.9	0.05	47	0.99
	1/15	0	8.3	0.07	46	0.98
	0	0	6.5	0.08	46	0.98
Pediatric	1/3	12.9	12.7	9.2	21	0.86
	4/15	13.0	6.4	6.7	26	0.98
	1/5	13.1	3.6	5.1	35	0.97
	2/15	13.2	2.3	4.0	38	0.97
	1/15	13.3	1.5	3.2	39	0.97
	0	13.4	1.0	2.7	40	0.97

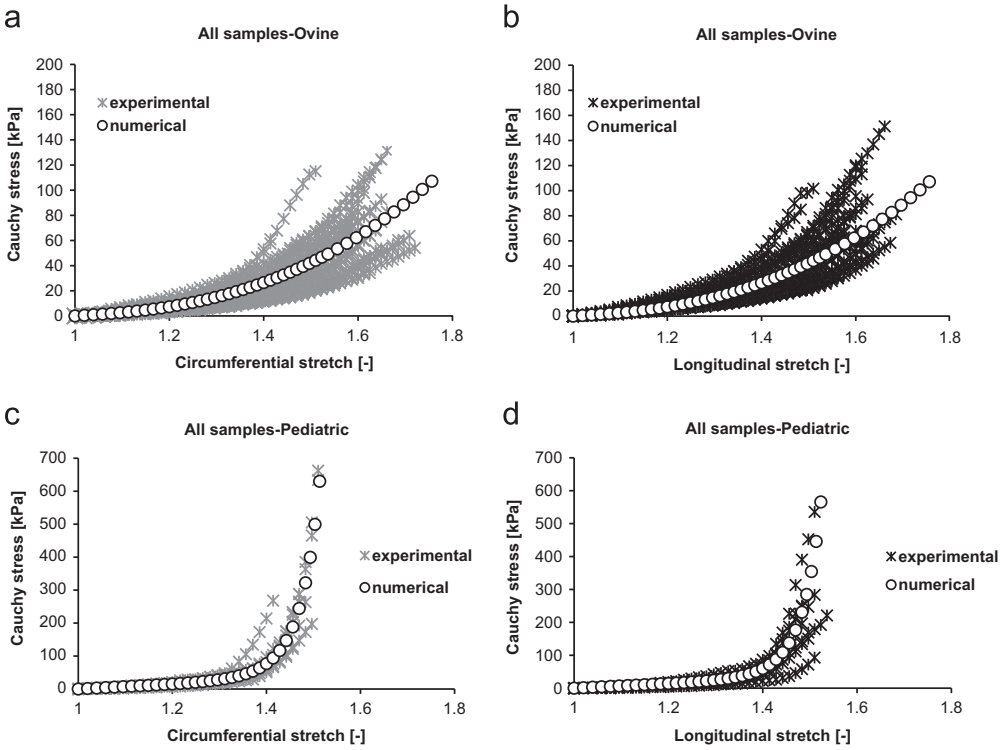

Fig. 7. All experimental stress-stretch curves and fitting results (a) ovine circumferential, (b) ovine longitudinal, (c) pediatric circumferential and (d) pediatric longitudinal. The numerical approximation was in close accordance with the experimentally determined results.

advanced. No histological or biochemical analysis of the tissue has been performed so far. The differences found between ovine and human pulmonary artery tissue may be related to their biochemical content, although this has not been assessed.

It should also be taken into account that we did not perform a microscopic study to assess the potential damage that could have occurred during sample preparation. It is possible that the cutting procedure could have induced tissue damage at the edge of the squared samples. However, the authors consider that our region of study is located far away from the extremities. The ovine samples were tested fresh and stored at 4 °C, whereas the pediatric artery was stored at −80 °C. There is no clear agreement about the influence of sample storage and freeze-thaw procedures on the mechanical properties of arteries. Some authors reported a different mechanical behavior between fresh and cryopreserved samples (Chow and Zhang, 2011; Venkatasubramanian et al., 2010). On the contrary, other studies have shown that cryopreservation does not modify the biomechanical properties of human arteries (Delgadillo et al., 2010; Bia et al., 2006). We compared the outcomes of biaxial tests performed on ovine samples stored at 4 °C and repeated the tests on samples from the same subject stored at −80 °C and the difference was not statistically significant. Finally, the parameters that are associated with the structure of the material are treated as phenomenological values in this study. Our next step will be to apply the parameters obtained in the present work to ovine and pediatric computational models to evaluate the response of a stent design in both environments.

5. Conclusion

A significant difference in mechanical properties between ovine and pediatric pulmonary artery tissue was observed when performing equibiaxial tensile tests. Ovine pulmonary arteries are more compliant and isotropic with a linear stress–strain behavior up to 26% strain, and have a higher thickness. On the other hand, pediatric tissue presented an anisotropic and strain-stiffening non-linear behavior, being stiffer in the circumferential direction. These differences were found to be significant beyond the physiological range and should be taken into account when modeling arterial tissue for testing stents for pre-clinical trials or when considering specific designs for pediatric applications. Moreover, care should be taken when comparing human tissue with ovine animal models for stent design purposes. The mechanical properties of ovine tissue presented in the present work might not be representative for human adult (50 ± 12 years) or pediatric (8 months) pulmonary arteries.

Conflict of interest statement

No financial support from other organizations, unless cited in the acknowledgments section nor personal relationships, nor people, nor organisms biased the development of this research work.

Acknowledgments

We would like to thank Bart Sanders for his contribution during tissue harvesting and transportation. The research leading to these results has received funding from the [European Community's] [European Atomic Energy Community's] Seventh Framework Programme ([FP7/2007-2013] [FP7/2007-2011]) under Grant agreement no. 242008.

References

Alastrué, V., Peña, E., Martínez, M., Doblaré, M., 2008. Experimental study and constitutive modelling of the passive mechanical properties of the ovine infrarenal vena cava tissue. Journal of Biomechanics 41, 3038–3045.

Attmann, T., Jahnke, T., Quaden, R., Boening, A., Muller-Hulsbeck, S., Cremer, J., Lutter, G., 2005. Advances in experimental percutaneous pulmonary valve replacement. The Annals of Thoracic Surgery 80, 969–975.

Auricchio, F., Di Loreto, M., Sacco, E., 2001. Finite-element analysis of a stenotic artery revascularization through a stent insertion. Computer Methods in Biomechanics and Biomedical Engineering 4, 249–264.

Azadani, A.N., Chitsaz, S., Matthews, P.B., Jaussaud, N., Leung, J., Wisneski, A., Ge, L., Tseng, E.E., 2011. Biomechanical comparison of human pulmonary and aortic roots. European Journal of Cardio-Thoracic Surgery 41, 1111–1116.

Bia, D., Pessana, F., Armentano, R., Pérez, H., Graf, S., Zócalo, Y., Saldías, M., Perez, N., Alvarez, O., Silva, W., Machin, D., Sueta, P., Ferrin, S., Acosta, M., Alvarez, I., 2006. Cryopreservation procedure does not modify human carotid homografts mechanical properties: an isobaric and dynamic analysis. Cell and Tissue Banking 7 (3), 183–194.

Chemla, D., Castelain, V., Provencher, S., Humbert, M., Simonneau, G., Hervé, P., 2009. Evaluation of various empirical formulas for estimating mean pulmonary artery pressure by using systolic pulmonary artery pressure in adults. Chest 135, 760–768.

Chow, M.J., Zhang, Y., 2011. Changes in the mechanical and biochemical properties of aortic tissue due to cold storage. Journal of Surgical Research 171, 434–442.

Conti, M., Auricchio, F., De Beule, M., Verhegghe, B., 2009. Numerical simulation of nitinol peripheral stents: from laser-cutting to deployment in a patient specific anatomy. In: Proceedings of ESOMAT 2009—8th European Symposium on Martensitic Transformations, Czech Republic, Prague.

Christie, G.W., Barratt-Boyes, B.G., 1995. Mechanical properties of porcine pulmonary valve leaflets: how do they differ from aortic leaflets? The Annals of Thoracic Surgery 60, 195–199.

Delgadillo, J.O.V., Delorme, S., El-Ayoubi, R., DiRaddo, R., Hatzikiriakos, S.G., 2010. Effect of freezing on the passive mechanical properties of arterial samples. Journal of Biomedical Science and Engineering 3, 645–652.

Fata, B., Carruthers, C.A., Gibson, G., Watkins, S.C., Gottlieb, D., Mayer, J.E., Sacks, M.S., 2013. Regional structural and biomechanical alterations of the ovine main pulmonary artery during postnatal growth. Journal of Biomechanical Engineering 135 (2), 021022, http://dx.doi.org/10.1115/1.4023389.

Fukui, T., Matsumoto, T., Tanaka, T., Ohashi, T., Kumagai, K., Akimoto, C., Tabayashi, K., Sato, M., 2005. In vivo mechanical properties of thoracic aortic aneurysmal wall estimated from in vitro biaxial test. Bio-Medical Materials and Engineering 15, 295–305.

Gao, Y., Raj, J.U., 2010. Regulation of the pulmonary circulation in the fetus and newborn. Physiological Reviews 90, 1291–1335.

Gasser, T.C., Ogden, R.W., Holzapfel, G.A., 2006. Hyperelastic modelling of arterial layers with distributed collagen fibre orientations. Journal of the Royal Society Interface 3, 15–35.

Geers, M.G.D., De Borst, R., Brekelmans, W.A.M., 1996. Computing strain fields from discrete displacement fields in 2D-solids. International Journal of Solids and Structures 33, 4293–4307.

Gozna, E.R., Marble, A.E., Shaw, A., Holland, J.G., 1974. Age-related changes in the mechanics of the aorta and pulmonary artery of man. Journal of Applied Physiology 36, 407–411.

Kao, P.H., Lammers, S., Tian, L., Hunter, K., Stenmark, K.R., Shandas, R., Qi, J.H., 2011. A microstructurally-driven model for pulmonary artery tissue. Journal of Biomechanical Engineering 133 (5), 1–37.

Kumar, G.P.V., Mathew, L., 2008. Effects of stent design parameters on the aortic endothelium. In: Proceedings of the 13th International Conference on Biomedical Engineering, Singapore, 23. pp. 1539–1542.

Laborde, J.C., Borenstein, N., Behr, L., Farah, B., Fajadet, J., 2005. Percutaneous implantation of an aortic valve prosthesis. Catheterization and Cardiovascular Interventions 65, 171–174.

Lally, C., Reid, A.J., Prendergast, P.J., 2004. Elastic behavior of porcine coronary artery tissue under uniaxial and equibiaxial tension. Annals of Biomedical Engineering 32 (10), 1355–1364.

Madhavan, K., Belchenko, D., Motta, A., Tan, W., 2010. Evaluation of composition and crosslinking effects on collagen-based composite constructs. Acta Biomaterialia 6, 1413–1422.

Marelli, A.J., Mackie, A.S., Ionescu-Ittu, R., Rahme, E., Pilote, L., 2007. Congenital heart disease in the general population: changing prevalence and age distribution. Circulation 115, 163–172.

Metzner, A., Stock, U.A., Iino, K., Fischer, G., Huemme, T., Boldt, J., Braesen, J.H., Bein, B., Renner, J., Cremer, J., Lutter, G., 2010. Percutaneous pulmonary valve replacement: autologous tissue-engineered valved stents. Cardiovascular Research 88, 453–461.

Pham, T., Sun, W., 2012. Comparison of biaxial mechanical properties of coronary sinus tissues from porcine, ovine and aged human species. Journal of Mechanical Behavior of Biomedical Materials 6, 21–29.

Roger, V.L., Go, A.S., Lloyd-Jones, D.M., Adams, R.J., Berry, J.D., et al., 2011. Heart disease and stroke statistics-2011 update: a report from the American Heart Association. Circulation 123, e18–e209.

Schievano, S., Taylor, A.M., Capelli, C., Lurz, P., Nordmeyer, J., Migliavacca, F., Bonhoeffer, P., 2010. Patient specific finite element analysis results in more accurate prediction of stent fractures: application to percutaneous pulmonary valve implantation. Journal of Biomechanics 43, 687–693.

Sirois, E., Wang, Q., Sun, W., 2011. Fluid simulation of a transcatheter aortic valve deployment into a patient-specific aortic root. Cardiovascular Engineering and Technology 2 (3), 186–195.

Sommer, G., Holzapfel, G.A., 2012. 3D constitutive modeling of the biaxial mechanical response of intact and layer-dissected human carotid arteries. Journal of the Mechanical Behavior of Biomedical Materials 5, 116–128.

Stephens, E.H., Grande-Allen, K.J., 2007. Age-related changes in collagen synthesis and turnover in porcine heart valves. Journal of Heart Valve Disease 16, 672–682.

Tzamtzis, S., Viquerat, J., Mullen, M.J., Burriesci, G., 2013. Numerical analysis of the radial force produced by the Medtronic-CoreValve and Edwards-SAPIEN after transcatheter aortic valve implantation (TAVI). Medical Engineering & Physics 35, 125–130.

Ussia, G.P., Barbanti, M., Tamburino, C., 2010. Management of percutaneous self-expanding bioprosthesis migration. Clinical Research in Cardiology 99, 673–676.

Venkatasubramanian, R.T., Wolkers, W.F., Shenoi, M.M., Barocas, V.H., Lafontaine, D., Soule, C.L., Iaizzo, P.A., Bischof, J.C., 2010. Freeze-thaw induced biomechanical changes in arteries: role of collagen matrix and smooth muscle cells. Annals of Biomedical Engineering 38, 694–706.

Wang, Q., Sirois, E., Sun, W., 2012. Patient-specific modeling of biomechanical interaction in transcatheter aortic valve deployment. Journal of Biomechanics 45 (11), 1965–1971.

Watanabe, H., Ohashi, K., Takeuchi, K., Yamashita, K., Yokoyama, T., Tran, Q., Satoh, H., Terada, H., Ohashi, H., Hayashi, H., 2002. Sildenafil for primary and secondary pulmonary hypertension. Clinical Pharmacology & Therapeutics 71, 398–402.

Wu, W., Qi, M., Liu, X., Yang, D., Wang, W., 2007. Delivery and release of nitinol stent in carotid artery and their interactions: a finite element analysis. Journal of Biomechanics 40, 3034–3040.

Zhao, S., Gu, L., Froemming, S.R., 2011. Assessment of shape memory alloy stent deployment in a stenosed artery. Biomedical Engineering Letters 1, 226–231.